Journal of Interventional Cardiac Electrophysiology (2023) 66:301–310
https://doi.org/10.1007/s10840-022-01172-6

Gross anatomic relationship between the human left atrial appendage and the left ventricular summit region: implications for catheter ablation of ventricular arrhythmias originating from the left ventricular summit

M. Kuniewicz[1,2] · K. Budnicka[1] · M. Dusza[1] · N. Jakob[1] · N. Cholewa[1] · R. Defonseka[1] · M. Gosnell[1] · T. Wadhwa[1] · J. Walocha[1] · H. Dobrzynski[1,3] · M. Hołda[1,3,4]

Received: 13 October 2021 / Accepted: 25 February 2022 / Published online: 9 March 2022

Abstract

Purpose The left ventricular summit (LVS) is a source of difficult-to-treat arrhythmias because of anatomical limitations. The aim of this study was to perform detailed research of the left atrial appendage (LAA) anatomy of cadaveric hearts to analyze their complex anatomy and coverage of the LVS.

Methods and results Eighty human formalin fixed hearts (mean age 44.4 ± 15.5, 27.5% females) were investigated. Each LAA size, type, and its relationship to the LVS were analyzed, as well as possible access sites for mapping/ablating electrode. Four types of LAA were observed over two LVS sites that are either accessible or not. The highest coverage over an inaccessible LVS area was observed in the Broccoli type, followed by the Windsock then the Chicken Wing and finally the Cactus types; over the accessible area of the LVS was observed in the Windsock, then in the Chicken Wing, then in the Cactus, and finally in the Broccoli types. The attainable coverage for electrode access is diminished from 25 to 65% because of the complex pectinate muscles and sharp angles. The highest density of the LAA floor made by pectinate muscles can be found in the Broccoli type ($p < 0.005$), while the Chicken Wing had the highest number of paper-thin-like pouches.

Conclusions The LAA appears to be a promising entry for ablation-qualified patients with the LV summit originate arrhythmias. The complex internal structure of the LAA may complicate ablation procedures. More prominent appendages are promising in more extensive mapping areas over the LVS.

Keywords Left atrial appendage · Left ventricular summit · Bipolar ablation · LAA · LVS

Abbreviations

BMI	Body mass index
BSA	Body surface area
Cx	Circumflex branch
Dg	Diagonal branch
EAT	Epicardial adipose tissue
GCV	Great cardiac vein
LA	Left atrium
LAA	Left atrial appendage
LAD	Left anterior descending artery
LCA	Left coronary artery
LV	Left ventricle
LVS	Left ventricular summit
OM	Obtuse marginal branch
PT	Pulmonary trunk
RFCA	Radiofrequency catheter ablation
SP	Septal perforator
VA	Ventricular arrhythmia

✉ M. Kuniewicz
kuniewiczm@gmail.com

1 Department of Anatomy, Jagiellonian University Medical College, Kopernika 12, 31-034 Cracow, Poland

2 Department of Electrocardiology, Institute of Cardiology, Jagiellonian University Medical College, Cracow, Poland

3 Division of Cardiovascular Sciences, The University of Manchester, Manchester, UK

4 HEART–Heart Embryology and Anatomy Research Team, Department of Anatomy, Jagiellonian University Medical College, Cracow, Poland

1 Introduction

Although the left atrial appendage (LAA) was originally thought to be a structural remnant of the developing heart with a minor physiological role, however, its significance in regulating hemodynamics and changes in cardiac rhythm suggests it may pay a more important role within therapeutic potentials and patients' benefits [1, 2]. The LAA is also responsible for triggering atrial fibrillation in patients who undergo more than one ablation therapies [3, 4]. Catheter ablation of idiopathic ventricular arrhythmias (VA) has shown high cure rates and is currently the first-line therapy; however, despite its advances, there is still a percentage of patients in which ablation cannot be successfully performed due to anatomic complexity and inaccessible areas to carry out these procedures. One of these inaccessible areas, bounded by the branches of the left coronary artery (LCA), is the left ventricular summit (LVS) [5]. Up to 14.5% of left VA may arise from the LVS [3, 6]. The catheter ablation from this region is successful in 83.6%; however, in long-term post-ablation, the procedural successful rate decreases to 68.1% [7]. Moreover, the complexity and incidence level of VAs are higher than those from different regions. Many important and fragile structures surround and pass through the LVS, making ablations challenging and unpredictable [5].

Anatomically, the LAA works as a favorable anatomical location for mapping and ablating arrhythmias arising from the LVS due to the large anatomical area that it covers [8]. The first successful radiofrequency (RF) ablation from the LAA was performed in 2002 [9]. In 2018, the LAA was described as a vantage point for mapping and ablating VAs originating from the LVS region in two case reports and bipolar RF catheter ablation (RFCA) in Japanese registry [10–12].

2 Anatomy of the LVS and LAA

The current study will explore the detailed anatomy of the external and internal aspects of the LAA and content of epicardial structures between the LAA and epicardial surface of the LVS.

The LVS is a triangular area located at the most superior part of the left epicardial ventricular region, surrounded by the two branches of the LCA: the left anterior interventricular artery and the left circumflex artery (Cx). The triangle is bounded by the apex, septal and mitral margins, and base [5]. The LVS is bisected by the great cardiac vein into an inaccessible area at its superior aspect and an accessible area at its inferior aspect [6, 8].

The LAA is a remnant of the primordial atrium, a finger-like extension originating from the main body at the most superior aspect within the LA. The LAA consists of the orifice, the neck, the body, and the lobes (Fig. 3). The entrance is known as the orifice and leads to the LAA neck overlapping the Cx branch of the LCA. The neck, which is a flattened in shaped structure, has its proximal margin/border located close to the LCA bifurcation, its distal margin/border located close to the Coumadin ridge, and its central aspect in the midline [13, 14]. The internal structures are lined by the pectinate muscle bundles that do not ramify like the teeth of a comb. The wall of the appendage is a paper-thin structure between the muscle bundles and provides undisrupted accessibility of mapping and ablation sites [14, 15].

3 Methods

We examined 80 dissected human hearts of cadaveric individuals who died of noncardiac causes. Demographic information of cadavers was acquired from the Jagiellonian University records for the donor's height, weight, age, sex, and LAA morphology.

Organs were collected during routine forensic medical autopsies. All hearts were dissected from adults ($n=22$; 27.5% were female whose mean age was 41.6 ± 11.5; and $n=58$; 72.5% were males whose mean age was 44.9 ± 16.1). The average body mass index (BMI) was 26.1 kg/m^2, and the mean heart weight was 442.0 ± 91.2 g. The leading causes of death were suicide, murder, and traffic/home accidents.

The hearts from the donors with known severe anatomic defects, past cardiac surgeries/interventions, or vascular or cardiac pathologies detected during autopsy (aneurysms, storage diseases, trauma) were not included into this study.

Each heart, along with the great vessels (their proximal portions), was dissected from the thoracic cavity. After removing excess blood, all specimens were weighed using a 0.5 g precision electronic laboratory scale (SATIS, BSA-L Laboratory, Poland). Subsequently, each heart was placed in a 10% paraformaldehyde solution for a minimum of 2 months. The hearts' cavities were opened in a routine manner. The LVS region was prepared with epicardial adipose tissue (EAT) removal and left coronary artery branches were revealed (Fig. 1A, B).

It has to be pointed out that the presence of fat can impede lesion formation with RF energy. We have observed a significant amount of adipose tissue seen at the LVS region epicardially prior to EAT removal. Then, on the septal margin, the septal perforator (SP) was marked and measured from the bifurcation of the LCA and values were recorded (Fig. 1D). The SPs were characterized by size; if more than one was found within each anterior descending artery (LAD), the more prominent one was chosen for the LVS delimitation

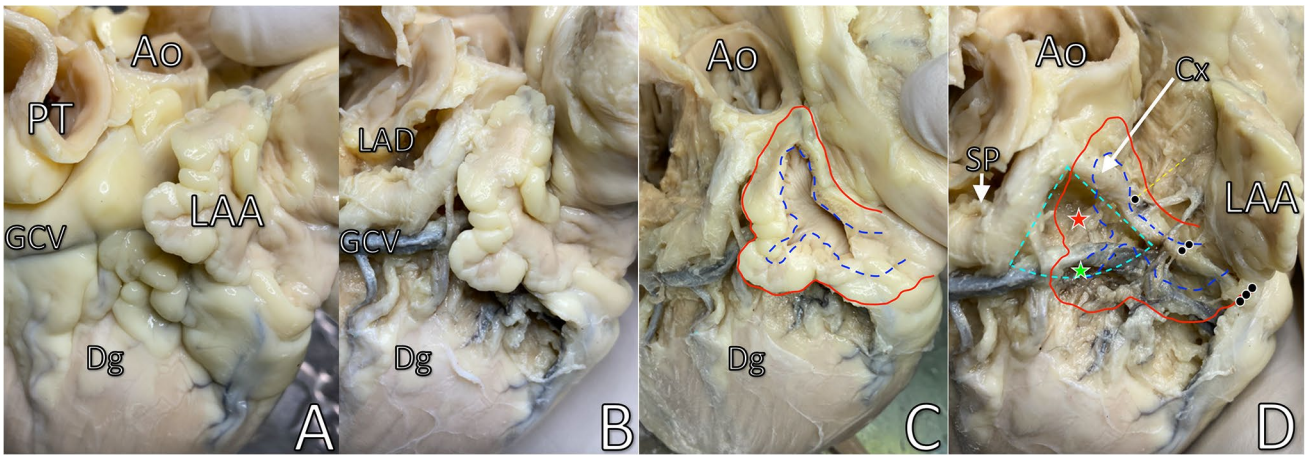

Fig. 1 Specimen preparation. **A** Heart with EAT over the LVS region. **B** After removal of EAT. **C** Opening the roof of the Cactus-shaped LAA; blue dotted line, internal coverage of the LAA over the LVS; red line, borders of the LAA covering the LVS region. **D** LVS after uplift of the LAA; red star, inaccessible area; green star, accessible area; single black dot, right border (proximal) of the LAA neck over mitral margin; double black dot, midline of the LAA neck; triple black dot, left border (distal) of the LAA neck over mitral margin. Abbreviations: Ao aorta, Cx circumflex branch, Dg diagonal branch, EAT epicardial adipose tissue, GCV great cardiac vein, LAA left atrial appendage, LAD left anterior descending artery, LVS left ventricular summit, PT pulmonary trunk, SP septal perforator

[5, 8]. The angle of bifurcation between the LAD and the circumflex branch (Cx) was measured with a protractor and values were recorded. The great cardiac vein was also mapped and both the accessible and inaccessible LVS areas were analyzed and measured.

The LAAs shape/type was assessed as previously described by Wang et al., Kimura et al., and Korhonen et al. [16–18]. In brief, the morphology of the LAA based on its 4 different physical shapes (Chicken Wing, Windsock, Cactus or Broccoli), and its measurements were recorded twice (before the incision of its external measurements and then after its roof was removed) (Fig. 2). Often, the morphology type/shape was changed after internal analysis was performed; therefore, the essential morphology was based on 3 criteria: (1) the LAA length (4 cm); (2) the interior angle between perpendicular line to the LAA orifice and line toward the tip of the LAA (100°); and (3) the lobe number. These 3 described criteria were necessary because of the complex internal LAA morphology, leading to significant discrepancies based just on its shape/type [19]. Nevertheless, the 4 shaped was used to simplify data illustration.

The external borders of the LAA neck were measured over the mitral LVS margin in accordance with its relationship to the Cx coronary artery (Fig. 1D): the proximal (the right border—a single black dot), the mid (the central part—a double black dot), and the distal (the left border—a triple black dot).

All LAA external dimensions were taken and included the number of lobes, lengths, and bend angles. After that, the roof of the LAA was removed, and the internal pectinate muscle framework was analyzed (Figs. 1C, 2) by counting the pectinate muscles at the base—the first visible separation of the pectinate muscle from the LAA floor before division into smaller branches (see white/blue asterisks in Fig. 2) [13, 14, 20, 21]. No muscles from the roof of the removed LAAs were taken into analysis. The gaps between the pectinate muscles were termed as "lacuna" or "pouch." Each pouch with a minimum of 3 mm width and 5 mm depth was taken into consideration as a potential recess for electrodes access (yellow asterisks, Fig. 3B). The electrode used for potential LAA ablation was the ThermoCool®SmartTouch™SF D-F curve as shown in Fig. 3B. The use of this particular electrode was to assess the potential accessibility inside the LAA for contact force electrodes. Finally, the distance between the LAA floor and the surface of the LVS was measured and values were recorded. Dissection in the midline of the LAA orifice (a double black dot on Fig. 1D and sagittal section on Fig. 3A) and the LA was performed to analyze the region between the LVS and the floor of the LAA (Fig. 3A).

For assessment of the LAA coverage over the LVS and the internal accessible surface, the Sketchandcalc© (iCalc Inc) computer software was used after a precise calibration (Fig. 4).

3.1 Statistical analysis

All variables were recorded as means and standard deviations. Correlational analysis between descriptive variables (e.g., age, sex, and BMI) and variables were assessed using the Pearson correlation method (r) with a significance set as $p < 0.05$. A chi-square test was used to evaluate difference in

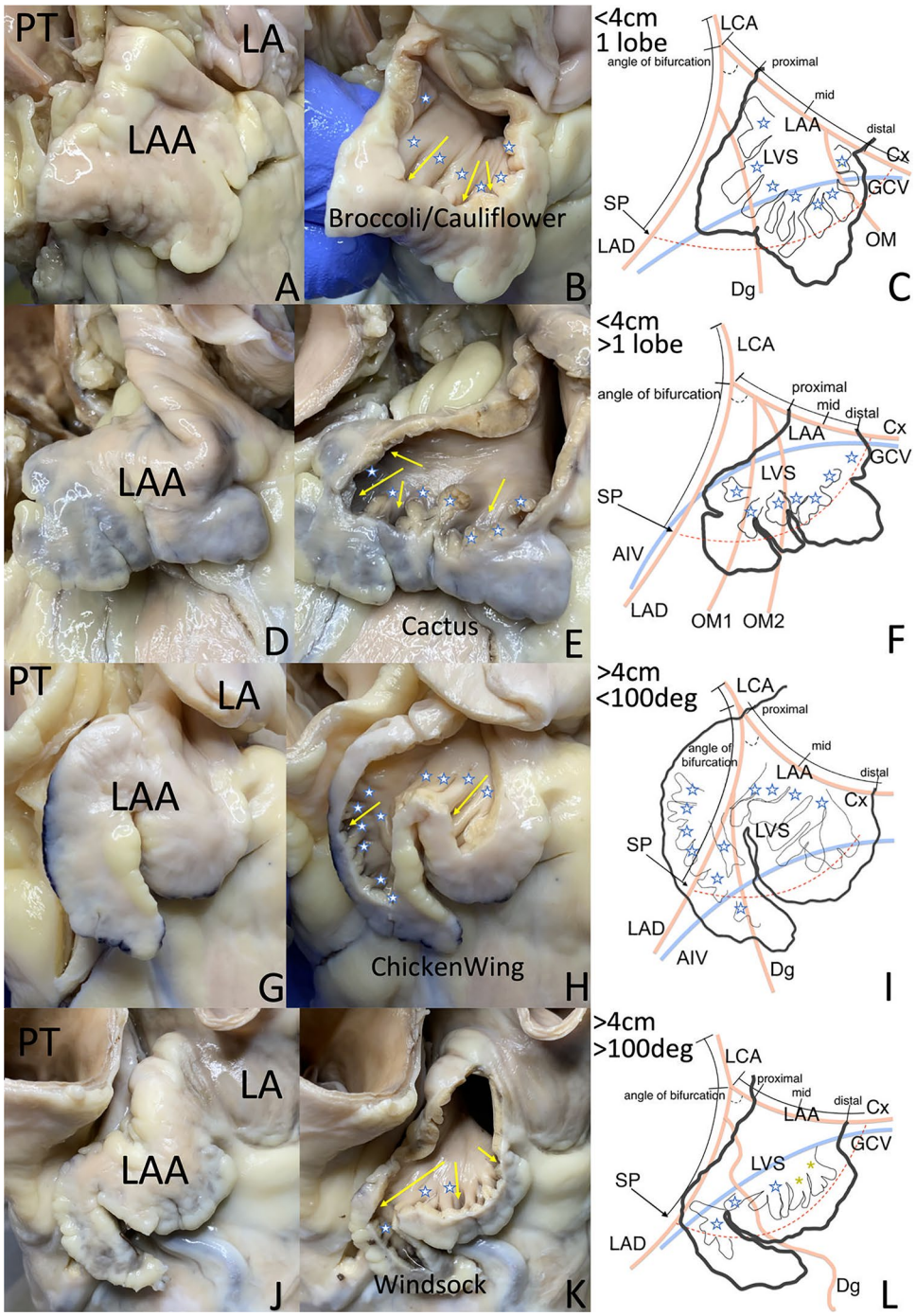

Fig. 2 Four shapes/types of the LAA and schematic illustration of relation to the LVS. White/blue asterisks indicate the origin of pectinate muscles. Yellow arrows point at lacunas/pouches attainable for electrode access. On schematic pictures, red dotted line is the margin of the LVS and black dotted line is the angle of the bifurcation. Abbreviations: Cx circumflex branch, Dg diagonal branch, GCV great cardiac vein, LA left atrium, LAA left atrial appendage, LAD left anterior descending artery, LCA left coronary artery, LVS left ventricular summit, OM obtuse marginal branch, PT pulmonary trunk, SP septal perforator, proximal, mid, and distal refer to the neck of the LAA

dichotomous data. The *t* test was used to evaluate difference in pectinate muscles density with a p value < 0.05 considered significant. All statistical analysis was conducted in STATISTICA v13.3 (Tibco CO) software ©.

4 Results

4.1 Analysis of external LAA data

Four LAA shapes/types were observed as illustrated in Fig. 2 and those shapes were Cactus, Windsock, Chicken Wing, and Broccoli. Their frequency of appearance in the explanted hearts investigated and relationships to age, weight, sex, and BMI were analyzed. The Windsock-shaped LAA in the

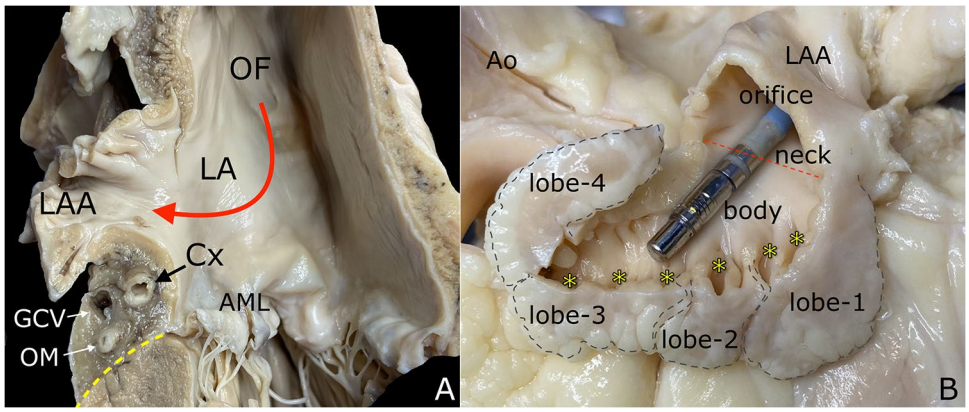

Fig. 3 **A** LAA seen from left atrium incision (big red curved arrow presents the course of the electrode from OF to the LAA and yellow dotted line is the LVS surface. **B** Illustrative electrode position inside the LAA (yellow asterisks indicate pouches/lacunas, red dotted line represents the neck part of the LAA). Abbreviations: AML anterior mitral leaflet, Ao aorta, GCV great cardiac vein, Cx circumflex branch, LA left atrium, LAA left atrial appendage, LVS left ventricular summit, OF oval fossa, OM obtuse marginal branch

cadaveric hearts had the highest frequency of appearance which was 36%, followed by the Chicken Wing (29%), the Cactus (21%), and the Broccoli (14%). The mean distance from the LCA bifurcation to the LAA proximal margin (at the right border of the LAA neck) was 3.13 mm, while to the distal part (the left border of the LAA neck) 22.05 mm (12.61–34.77 mm) (Fig. 1D). In 16 (20%) specimens out of total of 80 investigated, the LAA started at the point of the LCA bifurcation or reach this point immediately after. This occurred in 7 (24%) specimens of the Windsock-shaped LAA, 5 (22%) specimens of the Chicken Wing-shaped LAA, 3 (27%) specimens of the Broccoli-shaped LAA, and 1 (5%)

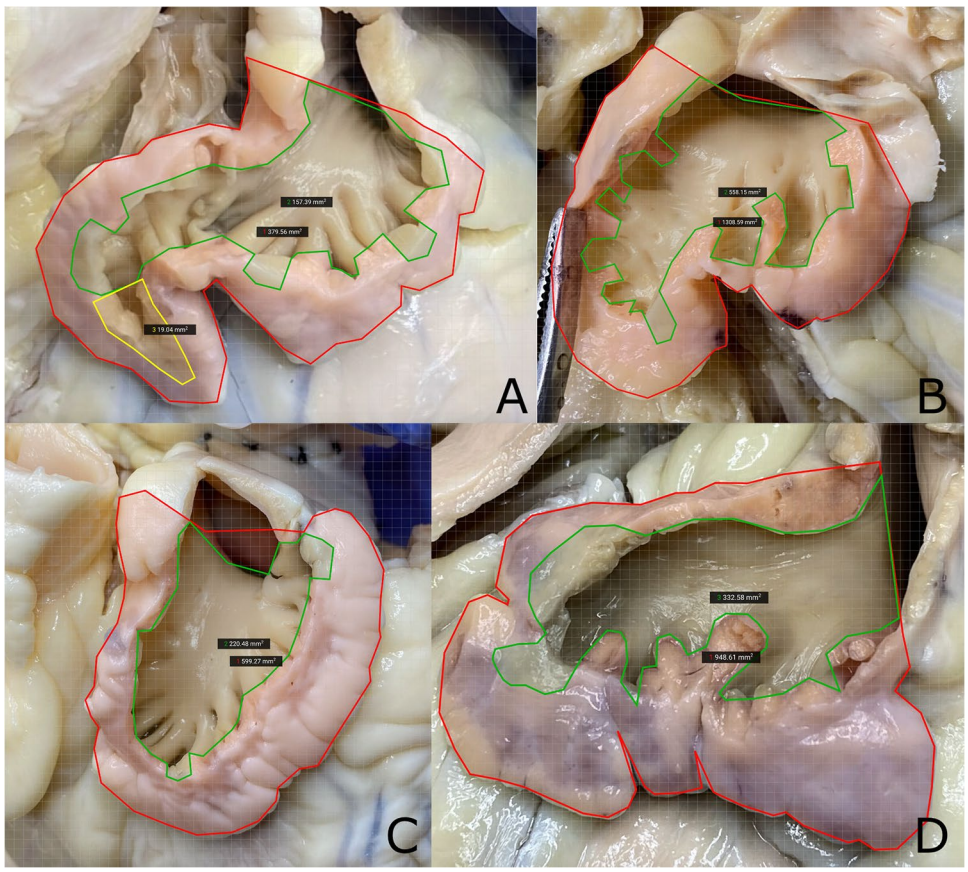

Fig. 4 Measurements of the "possible/safe" area for the LAA access in different types. Dimensions calculated with SketchAndCalc© (iCalc Inc) computer software. **A** Chicken Wing, **B** Windsock, **C** Broccoli, **D** Cactus. Red line—indicates the area of the LAA margins. Green area—possible electrode access inside appendage. Yellow line—open tip of the appendage inaccessible for used type mapping electrode

Table 1 Measurements of the external features of the LAA and coverage over the LVS in each type of LAA. *LAA prox*, proximal (right border of the LAA neck, single black dot in Fig. 1D); *Dist*, distal (left border of LAA neck, triple black dot in Fig. 1D); *Inf*, inferior; *Sup*, superior

	N = 80 hearts (100%)	Lobes of the LAA (n)	LAA neck prox margin–distal margin ± SD (mm)	Angles of the LAA axis ± SD (deg)	Length of the LAA ± SD (mm)	LAA area (mm^2) ± SD	Coverage over superior aspect LVS (%) ± SD	Coverage over inferior aspect LVS (%) ± SD
Chicken Wing	23 [29%]	1.00	2.44 ± 1.94 22.14 ± 5.07	89.21 ± 11.03 Min: 60 Max: 100	49.97 ± 8.50 Min: 40.50 Max: 75.30	606.31 ± 179.52 Min: 265 Max:1203	74.09 ± 21.09 *r* = 0.50 ***p* = 0.015**	56.55 ± 28.77 *r* = 0.42 ***p* = 0.046**
Windsock	29 [36%]	1.14 ± 0.58	3.06 ± 2.71 21.93 ± 3.42	142.93 ± 24.58 Min: 110 Max: 170	46.91 ± 6.74 Min: 40 Max: 69	519.96 ± 113.06 Min: 312 Max: 860	81.61 ± 16.25 *r* = − 0.14 *p* = 0.47	77.74 ± 30.70 *r* = − 0.08 *p* = 0.68
Broccoli	11 [14%]	1.00	4.17 ± 3.02 23.1 ± 3.23	154.27 ± 25.04 Min: 90 Max: 180	24.24 ± 3.96 Min: 18.20 Max: 29.30	330.56 ± 88.62 Min:172 Max: 521	89.30 ± 11.04 *r* = − 0.30 *p* = 0.37	34.09 ± 38.93 *r* = 0.42 *p* = 0.2
Cactus	17 [21%]	2.59 ± 0.79	3.48 ± 2.64 21.59 ± 2.68	141.18 ± 22.60 Min: 95 Max: 170	31.48 ± 3.72 Min: 24.70 Max: 36.15	419.01 ± 123.22 Min: 221 Max: 709	64.45 ± 21.31 *r* = 0.24 *p* = 0.35	45.52 ± 31.26 *r* = − 0.23 *p* = 0.37

specimen of the Cactus-shaped LAA (Fig. 2I). There was no correlation with any shape of the LAA vs. sex, BMI, BSA, or length of the appendage. The biggest mean area of the LAA was found in the Chicken Wing shaped which was 606.31 mm^2, followed by the Windsock shaped (519.97 mm^2), then the Cactus shaped (419.1 mm^2), and the smallest in the Broccoli shaped (330.56 mm^2). All data of the external measurements are shown in Table 1.

4.2 Analysis of internal LAA data

After dissection of the roof of the LAA, the number of the pectinate muscles was counted (see white/blue asterisks in Fig. 2) as described in the "Methods" section. Measurements of the internal features of the LAA are shown in Table 2. The largest number of the pectinate muscles and largest appendage were found in the Chicken Wing-shaped LAA (8.8 pectinate muscles/appendage), but there was no correlation between the size of the LAA and the number of the pectinate muscles. The smallest appendage was observed in the Broccoli-shaped LAA (7.7 pectinate muscles/appendage), followed by the Cactus shaped (7.6 pectinate muscles/appendage) and Windsock (6.8 pectinate muscles/appendage). In terms of a "density" ratio (i.e., the pectinate muscle per the total LAA area) for each appendage investigated, the highest ratio was found in the Broccoli type (0.025), followed by the Cactus type (0.02), then the Windsock (0.014), and lastly by the Chicken Wing (0.015). The statistical significance of the density ratio was found between the Broccoli to the Windsock type ($p < 0.005$) and the Broccoli to the Chicken Wing type ($p < 0.005$).

In the LAA, we have also investigated lacunas/pouches using 8.5F (3.0 mm) electrodes to determine access for the ablation catheter (Fig. 3B). Smaller pouches were not taken into consideration. The highest number of the accessible lacunas (min 3 mm width and 5 mm depth) was found in the Chicken Wing type ($n = 2.9$) and the Cactus type ($n = 2.4$), while the Windsock ($n = 1.9$) and the Broccoli type ($n = 1.3$) had the smallest number of the accessible lacunas (Table 2). We created maps of accessible areas inside the LAA (Fig. 4). In Fig. 4A, we classified the "pink" area as the inaccessible LAA areas due to the shape of the ablation catheter. Another obstacle that may prevent safe accessibility of the LAA is the possible second internal reverse torque. Even for a bidirectional electrode in vivo, some areas may not be able to be reachable to ablate. After computing the accessible

Table 2 Measurements of the internal features of the LAA. *Pectinate muscles, described in the method section; **Lacuna/pouch, min 3 mm width/5 mm depth. *LVS*, left ventricular summit

	N = 80 hearts (100%)	LAA orifice (horizontal ratio) [mm]	Pectinate muscles* [average n/LAA] (min–max)	Lacunas** (*n*)	Inaccessible internal area (Fig. 4)	Distance LAA- LVS (mm)
Chicken Wing	23 [29%]	19.69 ± 5.20	8.80 ± 3.10 (5–17)	2.90 ± 1.80	35–65%	5.32 ± 2.65
Windsock	29 [36%]	18.87 ± 2.90	6.80 ± 1.80 (5–11)	1.90 ± 1.50	25–45%	6.75 ± 3.41
Broccoli	11 [14%]	18.93 ± 4.60	7.70 ± 2.60 (5–12)	1.30 ± 0.70	30–60%	8.85 ± 2.16
Cactus	17 [21%]	18.11 ± 3.50	7.60 ± 4.30 (4–21)	2.40 ± 1.40	30–65%	6.21 ± 1.84

area inside the LAA using SkathandCalc, we found that the "real" in vivo access inside the LAA can be diminished from 25 to 65% according to the shape of the LAA (Fig. 4).

The LAA orifice length from the left atrium's vestibule into the appendage is almost similar in all shapes of the LAA (Table 2). The biggest size was recorded in the Chicken Wing type of the LAA (19.69 mm), followed by the Broccoli type (18.93 mm), then the Windsock type (19.87 mm), and finally in the Cactus type (18.11 mm). There was no correlation between the entrance orifice length and the length/area of the LAA in any type of the LAA (Table 2).

The only correlations observed was between the length of the LAA and the lacunas number in the Chicken Wing type ($r=0.44$ $p=0.04$) (Table 2). The LAA area to the lacunas number correlates in the Windsock type ($r=0.72$, $p=0.0001$) and the Cactus type ($r=0.75$, $p=0.0005$) (Table 2). The correlation between the number of the lobes and the number of the lacunas was only found in the Cactus type ($r=0.55$, $p=0.02$) (Table 2).

4.3 Relationship between LAA and LVS

The mean distance between the LAA floor and surface of the LVS was 6.3 ± 2.55 mm (2.8–12.2 mm min–max) (Table 2). According to the LAA type, the biggest distance was in the Broccoli type (8.85 ± 2.16 mm), followed by the Windsock type (6.75 ± 3.41 mm), then the Cactus type (6.21 ± 1.84 mm), and finally the Chicken Wing type (5.32 ± 2.65 mm). The distance was taken in a central aspect of the LAA body; however, it has to be noted that the LAA floor and the EAT thickness are not distributed equally in different types of the LAA (e.g., see Fig. 3A). As already mentioned above, the densest floor/density ratio (pectinate muscle/appendage) was found in the Broccoli and the Cactus LAA types.

The LVS area measurement was conducted by collecting the angle of the LCA bifurcation and the first dominant SP. Using Yamada's equation [8], the calculated LVS mean area size was 270.46 ± 160.21 mm^2. However, the size varied from 33.69 to 792.2 mm^2. The superior aspect mean value was from 162.23 ± 133.33 mm^2 and the inferior mean value was from 108.24 ± 108.67 mm^2.

The content of the LVS is highly variable. Only 11.25% (9 of 80 hearts) of the LVS were shown to have without trespassing the coronary arteries passing through them. The majority of the LVS contained at least one additional branch from the LAD (50 [62.5%] Dx branches in 80 hearts studied or 36 [45%] Cx branches in 80 hearts studied) and 16 specimens contained the ramus intermedius. Most (92.5%) of all LVS investigated comprise the GCV dividing the LVS into the superior and inferior fields. The relation of the LAA-LVS with additional coronary vessels is presented in Figs. 2, 1D, and 3B.

The biggest coverage over the superior aspect of the LVS was found in the Chicken Wing type, followed by the Windsock type, then the Cactus, and finally the Broccoli type (Table 1). We found that the highest coverage over the inaccessible area was in the Broccoli type (almost 90% of the inaccessible area) followed by the Windsock type (81.61%), then the Chicken Wing type (74.09%), and finally the Cactus type (64.45%).

The biggest coverage over inferior aspect of the LVS over the inferior area coverage was found in the Windsock type (77.74% of the accessible area), followed by the Chicken Wing type (56.55%), then in the Cactus type (45.52%), and finally in the Broccoli type (34.09%). The only correlation between the LAA size and the LVS coverage was found in the Chicken Wing type ($r=0.66$, $p=0.0006$) (Table 1).

There was no significant relationship between the LAA shape/type, percent coverage, sex, BMI, and cadaver weight. It is also worth reporting that the Chicken Wing type had the highest coverage over the septal summit and aorto-mitral continuity from the epicardial aspect.

5 Discussion

The anatomical relationship between the LAA and the LVS has previously been represented as case studies, registries, and imaging studies [5, 8–12]. In the current study, we conducted detailed analysis of a large sample of cadaveric hearts to investigate the LAA's coverage of the LVS and its usefulness in mapping and accessibility to ablate the arrhythmias arising from the LVS.

The LVS is bounded by two branches of the LCA bisected by the GCV. The superior inaccessible aspect is located above the GCV and can be reached from the epicardial side. It is covered by an extensive amount of EAT crossed by many coronary vessels. From an external approach, the LVS appears to be a narrow and delicate space for any clinical maneuvers. The inferior aspect lies below the coronary veins. According to electrophysiology studies, the most common point of arrhythmias in the LVS region is the transition between the GCV and the anterior interventricular vein also reachable from the epicardial side [22]. This region is also accessible from the venous system; however, the venous system may hinder a successful approach for ablation procedures [5]. It has been previously described that the LAA in 98% of human hearts cover the coronary venous transition point [8].

5.1 LAA coverage over LVS

The most common morphology amongst investigated hearts in our study was the Windsock and the Chicken Wing types. Both morphologies with the length of more than

4 cm represent approximately 2/3 of all samples. The mean biggest LAA area (measured by the external borders) was found to be in the Chicken Wing type (606.31mm^2) and was almost twice as big as the area obtained in the Broccoli type (330.56mm^2).

Interestingly, we found that the overall size of the LAA was not the ultimate indicator for degree of overlap with the LVS. Because of different angles and shapes, smaller appendages may have a bigger coverage in some parts of the LVS. For example, the Broccoli covers the most part of the inaccessible/superior area, while the Windsock covers the most part of the accessible/inferior of area of the LVS. The Chicken Wing (because of its sharp internal angle) provides the most coverage over the LVS, including the right ventricular output truck.

The overall size of the LVS, depending on the anatomy of the SP, and the coronary vein course are also highly variable amongst individuals [5].

5.2 LAA accessibility

While the external LAA borders, with a large coverage over the LVS, may be a promising vantage point for ablation of troublesome VAs, the internal LAA anatomy may bring obstacles. After removing the superior aspect of the LAA, we discovered that possible access to the LVS could be diminished from 25 to 65% from the external borders (Fig. 4). This is due to the sharp interior angles in a short distance, or the pectinate muscles may hinder access over desirable aspects. The pectinate muscles also arise in the central aspect of the LAA body and divide subsequent lobes (Fig. 2E). The number of the pectinate muscles, independently of the LAA type, may vary from 4 to 21; however, this is typically in a range from 5 to 9 in 64 hearts. The highest density (pectinate muscle/LAA area), and statistically significant ($p < 0.005$), of the pectinate muscles is observed in the Broccoli type, while the lowest density was found in the Chicken Wing type. The highest number of lacunas/pouches bigger than 3×5 mm/pouch was found in the Chicken Wing type (2.95/appendage) and the Cactus type (2.41/appendage) with statistical correlation of $p < 0.005$. Interestingly, the Cactus type has the highest number of penetrable pouches.

Some publications reported that extensivity of the trabeculation network within the LAA correlates with a higher rate of thromboembolic risk [23], while other did not find this correlation [19]. The Chicken Wing is possibly the most advantageous LAA of all types because it has the deepest and the most numerous lacunas. Meta-analytic studies indicate that patients with the Chicken Wing LAA morphology are less likely to develop thromboembolic events compared to those patients with other types of LAA morphologies. Specifically, patients with Broccoli morphologies were eight times more likely than Chicken Wing morphologies to experience stroke/transient ischemic attack events [23–25].

The Chicken Wing (because of at least one sharp angle) has smaller accessibility for catheter ablation; nevertheless, its large area size may compensate the internal access. The most accessible LAA type for the mapping electrode is the Windsock which offers a large coverage and no accessory lobes. The curvatures of the mapping electrodes also limit the possible approach; thus, the Windsock type is the most accessible LAA of all types.

5.3 LAA and LVS distance

The relationships of the LAA and the LVS in most individual clearly demonstrate the usefulness of the LAA as a vantage point for approaching the LVS when ablating arrhythmias arising from the supravalvular aortic to the septal summit region.

The presence of a base made up of fat tissue provides promising stability for adequate radiofrequency ablation energy delivery into target epicardial muscle tissue to safely target VA foci in a more controlled manner [26].

Unfortunately, the space between the LAA and the LVS (the inaccessible area) is a sensitive zone that contains the coronary artery branches from the left Cx artery or from the LAD; therefore, assessing the location of the cardiac vessels is crucial for procedural safety [6]. Thus, in patients undergoing ablation, pre-procedural imaging with computed tomography angiography may be helpful to assess the LAA morphology and its relationship to the LVS [17].

Lastly, the long LAA distance to the LVS surface, the LAA floor and EAT thickness, can also provide obstacles for performing ablation.

6 Limitations

There are a several limitations that are considered:

1. Cadaveric specimens were not surrounded by their physiological environment.
2. The body of the LAA with extending lobes into a complex and multiform structure is difficult to access. Therefore, the LAA access by electrodes (via a transseptal puncture) might be a pitfall and further anatomical research is needed to understand the possible mapping obstacles.
3. The muscle' density, which is highest in the Broccoli type, makes the floor of the LAA thick and thus may affect the measurements performed.
4. EAT size above the LVS is highly variable, and no correlation was found between BMI and BSA thickness.

5. EAT was removed before measurements were obtained. The presence of fat can impede lesion formation during RF delivery.
6. The autopsied hearts have smaller LAAs because they are not in their physiological state within the body and, e.g., have no circulatory blood volume flowing through them.

7 Conclusions

The LAA is the anatomical structure close to the left sinus of Valsalva, RVOT and pulmonary trunk, and the epicardial surface of the summit of the left ventricle. It is technically more accessible than the transvenous approach over the so-called Bermuda Triangle, which can only be completed in anatomically favorable patients [22, 26–29].

The Chicken Wing-shaped LAA has the best coverage over the septal summit region and projection over the right side of the LVS. The Windsock-shaped LAA is mostly accessible type; however, it is not covering the highest area of the LVS. The Cactus-shaped LAA contains the highest number of pouches and uprising pectinate muscles (in the central part of the body) and probably is the most sensitive type for access with the ablation catheter. The Broccoli-shaped LAA is the most robust for access with the ablation catheter but has a small range and thick inferior aspect therefore less applicable for RF/bipolar ablation.

Overall, the complex anatomy of the LAA provides helpful information on its accessibility to terminate troublesome arrhythmias originating from the LVS.

Author contribution M.K.: concept and design, anatomical dissections, photography, data collection, writing manuscript. B.K., D.M., J.N., C.N., D.R., G.M., W.T.: anatomical dissections, photography, data collection, English language support. H.D.: revising article critically for important intellectual content, English language support. M.H.: providing important intellectual content. J.W.: revising article critically for important intellectual content, final approval of submitted version. All authors have approved the final article.

Declarations

Ethics approval This study was conducted at the Department of Anatomy of the Jagiellonian University Medical College and was approved by the Bioethical Committee of the Jagiellonian University in Cracow, Poland (1072.6120.131.2018). The study protocol conformed to the ethical guidelines of the 1975 Declaration of Helsinki. The methods were carried out in accordance with the approved guidelines.

Conflict of interest The authors declare no competing interests.

References

1. Al-Saady NM, Obel OA, Camm AJ. Left atrial appendage: structure, function, and role in thromboembolism. Heart. 1999;82(5):547–54. https://doi.org/10.1136/hrt.82.5.547.PMID:10525506;PMCID:PMC1760793.
2. Regazzoli D, Ancona F, Trevisi N, Guarracini F, Radinovic A, Oppizzi M, Agricola E, Marzi A, Sora NC, Della Bella P, Mazzone P. Left atrial appendage: physiology, pathology, and role as a therapeutic target. Biomed Res Int. 2015;2015:205013. doi: https://doi.org/10.1155/2015/205013. Epub 2015 Jul 7. PMID: 26236716; PMCID: PMC4508372.
3. Hołda MK, Koziej M, Wszołek K, Pawlik W, Krawczyk-Ożóg A, Sorysz D, Łoboda P, Kuźma K, Kuniewicz M, Lelakowski J, Dudek D, Klimek-Piotrowska W. Left atrial accessory appendages, diverticula, and left-sided septal pouch in multi-slice computed tomography. Association with atrial fibrillation and cerebrovascular accidents. Kardiologia Polska 2018; 76, 3: 510–519; DOI: https://doi.org/10.5603/KP.a2018.0001
4. Saygi S. Atrial fibrillation and the role of LAA in pathophysiology and clinical outcomes? J Atr Fibrillation. 2012;5(3):480. https://doi.org/10.4022/jafib.480.PMID:28496767;PMCID:PMC5153207.
5. Kuniewicz M, Baszko A, Ali D, Karkowski G, Loukas M, Walocha JA, Hołda MK. Left ventricular summit-concept, anatomical structure and clinical significance. Diagnostics (Basel). 2021;11(8):1423. https://doi.org/10.3390/diagnostics11081423.PMID:34441357;PMCID:PMC8393416.
6. Yamada T, Doppalapudi H, Murakami Y, Yoshida Y, Yoshida N, Okada T, Tsuboi N, Inden Y, Murohara T, Epstein AE, Plumb VJ, Singh SP, Neal Kay G. Idiopathic ventricular arrhythmias originating from the aortic root prevalence, electrocardiographic and electrophysiologic characteristics, and results of radiofrequency catheter ablation. 2008; 52(2) 139–147. J. Am. Coll. Cardiol. https://doi.org/10.1016/j.jacc.2008.03.040
7. Chung FP, Lin CY, Shirai Y, Futyma P, Santangeli P, Lin YJ, Chang SL, Lo LW, Hu YF, Chang HY, Marchlinski FE, Chen SA. Outcomes of catheter ablation of ventricular arrhythmia originating from the left ventricular summit: a multicenter study. Heart Rhythm. 2020;17(7):1077–83. https://doi.org/10.1016/j.hrthm.2020.02.027 (**Epub 2020 Feb 28 PMID: 32113894**).
8. Kuniewicz M, Krupiński M, Gosnell M, Budnicka K, Jakob N, Karkowski G, Urbańczyk-Zawadzka M, Lelakowski J, Walocha J. Applicability of computed tomography preoperative assessment of the LAA in LV summit ablations. J Interv Card Electrophysiol. 2021 Aug;61(2):357–363. doi: https://doi.org/10.1007/s10840-020-00817-8. Epub 2020 Jul 14. PMID: 32666410; PMCID: PMC8324620.
9. Sosa E, Scanavacca M, d'Avila A. Catheter ablation of the left ventricular outflow tract tachycardia from the left atrium. J Interv Card Electrophysiol. 2002;7:61–5.
10. Benhayon D, Cogan J, Young M. Left atrial appendage as a vantage point for mapping and ablating premature ventricular contractions originating in the epicardial left ventricular summit. 2018; 6(6):1124-1127; https://doi.org/10.1002/ccr3.1525
11. Yakubov A, Salayev O, Hamrayev R, Sultankhonov S. A case of successful ablation of ventricular tachycardia focus in the left ventricular summit through the left atrial appendage: a case report. European Heart Journal - Case Reports. 2018;2(4):1–5. https://doi.org/10.1093/ehjcr/yty110.
12. Igarashi, M., Nogami, A., Fukamizu, S., Sekiguchi, Y., Nitta, J., Sakamoto, N., … Ieda, M. (2020). Acute and long-term results of bipolar radiofrequency catheter ablation of refractory ventricular arrhythmias of deep intramural origin. *Heart Rhythm*,

13. Whiteman, S.; Saker, E.; Courant, E.; Salandy, S.; Gielecki, J.; Zurada, A.; Loukas, M. An anatomical review of the left atrium, Translational Research in Anatomy, 2019, Volume 17, 100052, ISSN 2214-854X, https://doi.org/10.1016/j.tria.2019.100052
14. Beigel R, Wunderlich NC, Ho SY, Arsanjani R, Siegel RJ. The left atrial appendage: anatomy, function, and noninvasive evaluation. JACC Cardiovasc Imaging. 2014;7(12):1251–65. https://doi.org/10.1016/j.jcmg.2014.08.009 (**PMID: 25496544**).
15. Su P, McCarthy KP, Ho SY. Occluding the left atrial appendage: anatomical considerations. Heart. 2008;94:1166–70. https://doi.org/10.1136/hrt.2006.111989.
16. Wang Y, Di Biase L, Horton RP, et al. Left atrial appendage studied by computed tomography to help planning for appendage closure device placement. J Cardiovasc Electrophysiol. 2010;21(9):973–82. https://doi.org/10.1111/j.1540-8167.2010.01814.x,indexedinPubmed:20550614.
17. Korhonen M, Parkkonen J, Hedman M, Muuronen A, Onatsu J, Mustonen P, Vanninen R, Taina M. Morphological features of the left atrial appendage in consecutive coronary computed tomography angiography patients with and without atrial fibrillation. PLoS ONE. 2017;12(3): e0173703. https://doi.org/10.1371/journal.pone.0173703.PMID:28288200;PMCID:PMC5348027.
18. Kimura T, Takatsuki S, Inagawa K, Katsumata Y, Nishiyama T, Nishiyama N, Fukumoto K, Aizawa Y, Tanimoto Y, Tanimoto K, Jinzaki M, Fukuda K. Anatomical characteristics of the left atrial appendage in cardiogenic stroke with low CHADS2 scores. Heart Rhythm 2013;10:921–925.*17*(9), 1500–1507.
19. Wu L, Liang E, Fan S, Zheng L, Du Z, Liu S, Hu F, Fan X, Chen G, Ding L, Yao Y. Relation of left atrial appendage morphology determined by computed tomography to prior stroke or to increased risk of stroke in patients with atrial fibrillation. Am J Cardiol. 2019;123(8):1283–6. https://doi.org/10.1016/j.amjcard.2019.01.024 (**Epub 2019 Jan 23 PMID: 30709597**).
20. Wang K, Ho SY, Gibson DG, Anderson RH. Architecture of atrial musculature in humans. Br Heart J. 1995;73(6):559–65. https://doi.org/10.1136/hrt.73.6.559.PMID:7626357;PMCID:PMC483920.
21. Ho SY, Cabrera JA, Sanchez-Quintana D. Left atrial anatomy revisited. Circ Arrhythm Electrophysiol. 2012;5(1):220–8. https://doi.org/10.1161/CIRCEP.111.962720,indexedinPubmed:22334429.
22. Obel, O. A., Avila, A., Neuzil, P., Saad, E. B., Ruskin, J. N., & Reddy, V. Y. (2006). *Ablation of left ventricular epicardial outflow tract tachycardia from the distal great cardiac vein*. Journal of the American College of Cardiology, *48*(9), 6–10. https://doi.org/10.1016/j.jacc.2006.06.006
23. Di Biase L, Santangeli P, Anselmino M, Mohanty P, Salvetti I, Gili S, Horton R, Sanchez JE, Bai R, Mohanty S, Pump A, Cereceda Brantes M, Gallinghouse GJ, Burkhardt JD, Cesarani F, Scaglione M, Natale A, Gaita F. Does the left atrial appendage morphology correlate with the risk of stroke in patients with atrial fibrillation? Results from a multicenter study. J Am Coll Cardiol. 2012;60(6):531–8. https://doi.org/10.1016/j.jacc.2012.04.032 (**PMID: 22858289**).
24. Lupercio F, Carlos Ruiz J, Briceno DF, et al. Left atrial appendage morphology assessment for risk stratification of embolic stroke in patients with atrial fibrillation: a meta-analysis. Heart Rhythm. 2016;13(7):1402–9. https://doi.org/10.1016/j.hrthm.2016.03.042.
25. Kimura T, Takatsuki S, Inagawa K, Katsumata Y, Nishiyama T, Nishiyama N, Fukumoto K, Aizawa Y, Tanimoto Y, Tanimoto K, Jinzaki M, Fukuda K. Anatomical characteristics of the left atrial appendage in cardiogenic stroke with low CHADS2 scores. Heart Rhythm. 2013;10(6):921–5. https://doi.org/10.1016/j.hrthm.2013.01.036 (**Epub 2013 Feb 4 PMID: 23384894**).
26. Enriquez A, Malavassi F, Saenz LC, Supple G, Santangeli P, Marchlinski FE, Garcia FC. How to map and ablate left ventricular summit arrhythmias. Heart Rhythm. 2017;14(1):141–8.
27. Altmann DR, Knecht S, Sticherling C, Ammann P, Osswald S, Kühne M. Ventricular tachycardia originating from the " Bermuda Triangle." Cardiovascular Medicine. 2013;16(7–8):208–10.
28. Żabówka A, Hołda J, Strona M, Koziej M, Krawczyk-Ożóg A, Jasińska KA, Kuniewicz M, Lelakowski J, Hołda MK. Morphology of the Vieussens valve and its imaging in cardiac multislice computed tomography. J Cardiovasc Electrophysiol. 2019;30(8):1325–9. https://doi.org/10.1111/jce.14018 (**Epub 2019 Jun 18 PMID: 31187551**).
29. Mazur M, Żabówka A, Bolechała F, Kopacz P, Klimek-Piotrowska W, Hołda MK. Variations and angulation of the coronary sinus tributaries: implications for left ventricular pacing. Pacing Clin Electrophysiol. 2019;42(4):423–30. https://doi.org/10.1111/pace.13618 (**Epub 2019 Feb 21 PMID: 30740749**).
30. Singh M, Edwards WD, Holmes DR Jr, Tajil AJ, Nishimura RA. Anatomy of the first septal perforating artery: a study with implications for ablation therapy for hypertrophic cardiomyopathy. Mayo Clin Proc. 2001;76(8):799–802 (**PMID: 11499819**).